Available online at www.sciencedirect.com
ScienceDirect
European Journal of Mechanics A/Solids 26 (2007) 854–871

Consistent thermodynamic modelling of wire-reinforced geomaterials

R. Laniel *, P. Alart, S. Pagano

LMGC, UMR CNRS 5508, Université Montpellier II, CC 048, Place Eugène Bataillon, 34095 Montpellier cedex 5, France

Received 30 May 2006; accepted 30 January 2007

Available online 13 March 2007

Abstract

The *TexSol* is a composite geomaterial: a sand matrix with a wire network reinforcement. For small strains a thermodynamic continuous model of the *TexSol* including the unilaterality of the wire network is postulated. This model is described by two potentials which depend on some internal variables and a state variable either strain or stress tensor (the choice of this last one gives two different ways of identification). The *TexSol* continuous model is implemented in a finite element code to retrieve the mechanical behaviour given by discrete element numerical experiments.

Keywords: Geomaterial; Unilaterality; Thermodynamics

1. Motivations

1.1. What is the TexSol?

The civil-engineering constructions need plane stable floor. The environment configuration often forces civil engineers to setup huge embankments. Moreover, it can be interesting to reinforce them to ensure a better embankment mechanical behaviour. A lot of different solutions can be used to reinforce soil but, in this paper, we focus our attention on the *TexSol* method.

The *TexSol*, created in 1984 by Leflaive Khay and Blivet from LCPC (Laboratoire Central des Ponts et Chaussées) (Leflaive et al., 1985), is a heterogeneous material obtained by mixing sand and wire network. This reinforced material has a higher strength than sand without wire. Of course, the *TexSol* behaviour depends on sand and wire parameters and its friction angle can be larger than sand by 0° to 10° (Khay and Gigan, 1990). The wire is described by its linear density in dtex units (1 dtex $= 10^{-7}$ kg m^{-1}), ponderal content and stiffness. Classically, the wire density in a *TexSol* sample ranges between 10^5 m^{-2} and 2×10^5 m^{-2}.

To make a *TexSol* bank, a machine named *"Texsoleuse"* is used. It proceeds by throwing sand and, at the same time, injecting wire. The wire is placed on the free surface of sand with random orientation. This machine carries out several passes to setup the bank. Fig. 1 represents the *TexSol* microstructure. In the literature, we find two different continuous

* Corresponding author. Tel.: +33 4 67 14 45 37.
E-mail address: romain.laniel@lmgc.univ-montp2.fr (R. Laniel).

0997-7538/$ – see front matter
doi:10.1016/j.euromechsol.2007.01.003

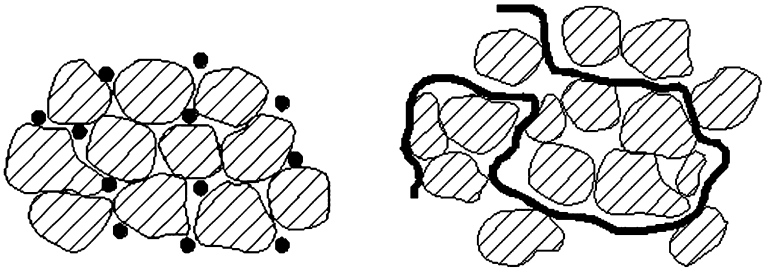

Fig. 1. Schematic *TexSol* sections.

modellings. The model suggested in (Fremond, 2002) is non-local and includes remote interactions (corresponding to the wire effects) but requires identification of their parameters using macroscopic experiments. Villard proposes a simpler local model in (Villard, 1988; Villard and Jouve, 1989). It couples a standard model of sand and an equivalent unilateral elastic stiffness contribution corresponding to the wire network. This last contribution is activated only on the tension directions because of the unilateral behaviour of wire. Our main work is to clearly define thermo-dynamical potentials of the Villard local model with both stress and strain formulations to identify the best-adapted one. Such a stage is useful before carrying out a homogenisation procedure applied to an untypical material. In the absence of physical experiments, the identification of macroscopic model will be performed using numerical experiments. In the paper we use the continuum mechanics conventions.

1.2. Assumptions of the continuous local model

To couple the elasto-plastic model of the sand and the unilateral elastic model of the wire network, we have to consider some mechanical assumptions, which may be backed by numerical experiments performed with a discrete elements software (Dubois and Jean, 2003; Moreau, 1999). We limit this study to the small strain framework; the stress tensor $\boldsymbol{\sigma}$ becomes a Cauchy stress tensor.

1.2.1. Stress additivity assumption

In this paper, the stress additivity assumption of sand and wire network is assumed. Then, we write

$$\boldsymbol{\sigma} = \boldsymbol{\sigma}_s + \boldsymbol{\sigma}_w, \tag{1}$$

where $\boldsymbol{\sigma}$, $\boldsymbol{\sigma}_s$ and $\boldsymbol{\sigma}_w$ are the second order stress tensors of the *TexSol*, sand and wire network, respectively.

This assumption seems to be consistent with the *TexSol* quasi-static behaviour. We can get a good approximation of the stress tensor in numerical simulation of 2D granular matter (Mouraille, 2004) using the Weber stress tensor (Cambou and Jean, 2001),

$$\boldsymbol{\sigma}_{\Omega} = \frac{1}{V_{\Omega}} \sum_{\alpha \in \Omega} l^{\alpha} \otimes r^{\alpha}.$$

This tensor is an average over a domain Ω of volume V_{Ω}, where l^{α} and r^{α} are the inter-center vector and the contact force vector of a contact α. It may be asymmetric if inertial effects are not negligible. For quasi-static processes this discrete tensor is a good candidate to represent a continuous stress tensor. Moreover, we can define such a tensor grain by grain with the approach of Moreau (Moreau, 1999). In this way, a wire network stress and a sand stress may be computed, to retrieve by addition the full *TexSol* stress (in the discrete simulation, the wire is modelled by a chain of beads with unilateral interactions, (Laniel et al., 2005)). In a biaxial test (deviatoric load on a confined material) computed with *LMGC90* using the Non Smooth Contact Dynamics method (Dubois and Jean, 2003; Jean, 1999), we check the symmetry of the stress tensor even at large strains as long as the process remains slow (no inertial effects).

In Fig. 2, we display the principal values of the Weber stress tensor (EV1, EV2), where the contributions of each components can be compared. The wire network is in tension and sand is in compression in both principal directions. These features may be also observed in the force network of granular samples.

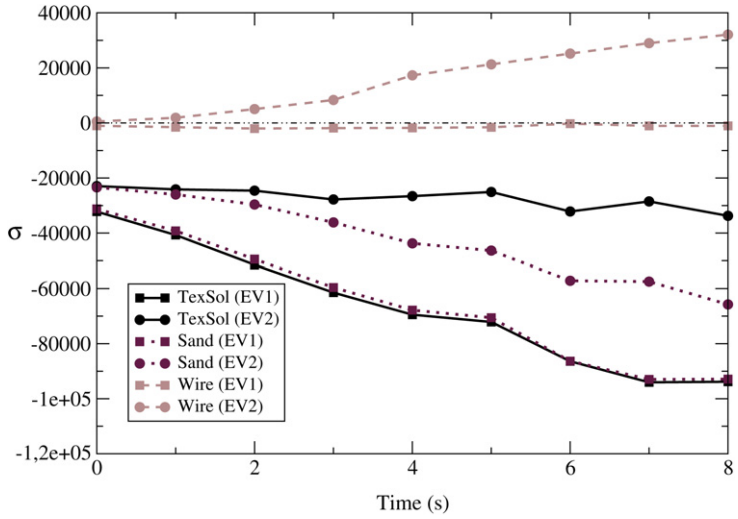

Fig. 2. Stress eigen values evolution in the *TexSol*.

1.2.2. Non-sliding assumption

This second assumption is not as evident as the previous one. Although micro slidings occur between sand grains and wire, we assume that at the macroscopic level of the continuum model, the sand network does not slip with respect to the wire network. This assumption can be written by the equality of the three strain rates,

$$\dot{\boldsymbol{\varepsilon}}_s = \dot{\boldsymbol{\varepsilon}}_w = \dot{\boldsymbol{\varepsilon}}, \tag{2}$$

where $\boldsymbol{\varepsilon}_s$, $\boldsymbol{\varepsilon}_w$ and $\boldsymbol{\varepsilon}$ are the second order strain tensor of the sand, wire network and *TexSol*, respectively.

We have to be very careful with such a condition and define some validity domains for it. Indeed, the limits of this assumption are difficult to quantify and we will restrict the validation of the following continuum model to small strains.

1.3. Role of the wire unilaterality

The wire network contributes to the tensile stiffness of the composite material but not to the compression stiffness (cf. Fig. 2). To model such a behaver at the macroscopic scale, it is convenient to introduce a unilateral condition in the behaviour law of the wire network. This unilaterality accounts for two microscopic phenomena. The first one is the lack of bending strength of the wire network viewed as a piece of cotton. The second one is the local buckling of short segments. The first aspect is not explicitly taken into account by a unilateral condition at the microscopic scale in our discrete numerical simulation since the chain of beads has no bending strength. The second aspect may be enforced by introducing a unilateral interaction law between two successive beads. Such an interaction models an elemental wire between two beads: we denote by "rigid wire"; otherwise, we will refer to it as "rigid rod" (cf. Fig. 4) for bilateral law between beads. Fig. 3 illustrates the difference of global behaviour between the two simulations for biaxial test using the *LMGC90* software. Until 6% of deformation, the responses are almost identical, for larger deformations the "rigid rod" model leads to a rough increase of stiffness due to the appearance of compressive columns in the wire. Such a phenomenon does not seem very realistic and stems probably from a scale effect since the numerical sample is not fully representative of the material. In particular, the model of wire as a chain of beads generates unrealistic jamming effect with sand grains.

1.4. Why strain and stress formulations?

In this paper, we propose to carry out a thermodynamic study with both strain and stress formulations. The interest of this work is in the identification possibilities of potentials parameters. Indeed, an experimenter performing tests on a sample has only access to the *global* strain. Our numerical investigations allow us to have access to finer data such

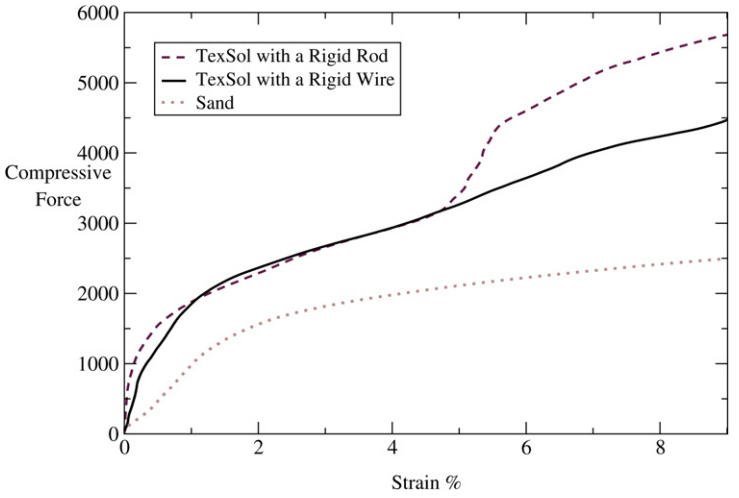

Fig. 3. Vertical force vs. vertical strain response with different models.

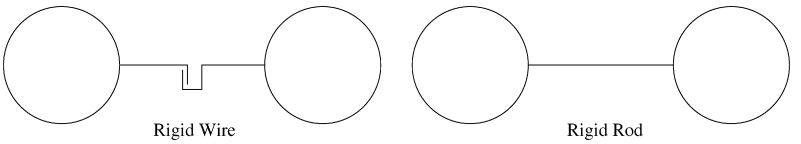

Fig. 4. Schematic discrete laws.

as the *local* stress field throughout the sample. Moreover, the *global* stress tensor over the sample can be deduced by averaging.

The post-processing of numerical experiments mentioned in Section 1.2.1 provides precise information on the stress fields in sand and wire network. The stress "unilaterality" in the wire is clearly established in Fig. 2. This observation could lead us to favour a stress formulation. But the finite element softwares are essentially developed using a strain formulation. Moreover, the unilaterality may be postulated either on the strain or on the stress according to the chosen approach. But these models are not dual of one another as we will see in the next section. Consequently, we propose in the following study strain formulations which are easily implementable. Dual stress formulations are provided when they can be analytically deduced by the Legendre–Fenchel transformation.

2. A general thermodynamic framework

In this part, we define potentials written with different state variables. These potentials have to satisfy the Clausius–Duhem inequality to be thermodynamically admissible. The notation conventions for an unspecified variable are X for a scalar or a vector, $\boldsymbol{X}$ for a second or third order tensor and $\mathbb{X}$ for a fourth or higher order tensor.

2.1. Strain versus stress approach in thermodynamics

This work must be as exhaustive as possible, when passing from unspecified state variables to its dual. We thus use the Legendre–Fenchel transformation (Moreau, 1966), to carry out our study with both strain and stress formulations. Let us write the Clausius–Duhem inequality where u is the internal energy, s the massic entropy, q the heat flow vector and T the temperature,

$$\boldsymbol{\sigma} : \dot{\boldsymbol{\varepsilon}} - \rho(\dot{u} - T\dot{s}) - \frac{1}{T} q \cdot \nabla T \geqslant 0, \tag{3}$$

where ∇ is the gradient operator. The intrinsic dissipation depends on a state variable $\boldsymbol{X}$ (or its dual $\boldsymbol{X}^*$), some internal variables $\alpha = \{\alpha_1, \ldots, \alpha_p\}$ (each internal variable can be scalar, vectorial or tensorial) and the temperature T.

It can also be expressed with the free energy ψ or its Legendre–Fenchel transformation ψ^* with respect to the state variable $\boldsymbol{X}$,

$$\psi(\boldsymbol{X},\alpha,T) = u(\boldsymbol{X},\alpha,T) - Ts(\boldsymbol{X},\alpha,T) \quad \text{and}$$
$$\psi^*(\boldsymbol{X}^*,\alpha,T) = \sup_{\overline{\boldsymbol{X}}}\left\{\overline{\boldsymbol{X}}\colon\ \boldsymbol{X}^* - \psi(\overline{\boldsymbol{X}},\alpha,T)\right\} = \boldsymbol{X}:\boldsymbol{X}^* - \psi(\boldsymbol{X},\alpha,T),$$

where $\boldsymbol{X}$ is the argument of the supremum. Considering either $\boldsymbol{X}$ or $\boldsymbol{X}^*$, we find two expressions of the Clausius–Duhem inequality,

$$\boldsymbol{\sigma}:\dot{\boldsymbol{\varepsilon}} - \rho\left[\frac{\partial\psi}{\partial\boldsymbol{X}}:\dot{\boldsymbol{X}} + \left(s + \frac{\partial\psi}{\partial T}\right)\dot{T} + \frac{\partial\psi}{\partial\alpha_m}\dot{\alpha}_m\right] - \frac{q}{T}\cdot\nabla T \geqslant 0, \tag{4}$$

$$\boldsymbol{\sigma}:\dot{\boldsymbol{\varepsilon}} - \rho\left[\dot{\boldsymbol{X}}:\boldsymbol{X}^* + \left(\boldsymbol{X} - \frac{\partial\psi^*}{\partial\boldsymbol{X}^*}\right):\dot{\boldsymbol{X}}^* + \left(s - \frac{\partial\psi^*}{\partial T}\right)\dot{T} - \frac{\partial\psi^*}{\partial\alpha_m}\dot{\alpha}_m\right] - \frac{q}{T}\cdot\nabla T \geqslant 0. \tag{5}$$

Using the Helmholtz postulate (which can be applied with the generalised standard materials assumption (Halphen and Nguyen, 1975)) and the previous definitions, we are now able to deduce the state laws,

$$\begin{array}{ll}
\text{Primal state laws} & \text{Dual state laws}\\
\boldsymbol{X}^* \in \partial_{\boldsymbol{X}}\psi(\boldsymbol{X},\alpha,T), & \boldsymbol{X} \in \partial_{\boldsymbol{X}^*}\psi^*(\boldsymbol{X}^*,\alpha,T),\\
-s \in \partial_T\psi(\boldsymbol{X},\alpha,T), & s \in \partial_T\psi^*(\boldsymbol{X}^*,\alpha,T),\\
-\dfrac{1}{\rho}A_m \in \partial_{\alpha_m}\psi(\boldsymbol{X},\alpha,T), & \dfrac{1}{\rho}A_m \in \partial_{\alpha_m}\psi^*(\boldsymbol{X}^*,\alpha,T),
\end{array} \tag{6}$$

where A_m is the thermodynamic force associated with α_m. Formally, we use subdifferentials instead of derivatives; for a function f at the point p it is defined by $\partial_p f = \{q \mid \forall r,\ f(r) - f(p) \geqslant q(r-p)\}$. If convexity is not required, previous relations still hold using the Clarke subdifferential (Clarke, 1983). Then, the primal and dual forms are not necessarily equivalent. In the general case, the Clausius–Duhem inequality (4) or (5) can be reduced to a dot product of a vector flow and a vector force,

$$\underbrace{\begin{bmatrix}\hat{\boldsymbol{\sigma}}\\ A\\ \nabla T\end{bmatrix}^{\mathrm{T}}}_{\text{force}} \cdot \underbrace{\begin{bmatrix}\dot{\hat{\boldsymbol{\varepsilon}}}\\ \dot{\alpha}\\ -\frac{q}{T}\end{bmatrix}}_{\text{flow}} \geqslant 0, \quad \text{where } \begin{cases}\dot{\hat{\boldsymbol{\varepsilon}}} = \dot{\boldsymbol{\varepsilon}} \text{ or } \dot{\boldsymbol{\varepsilon}}^{\mathrm{ir}},\\ \hat{\boldsymbol{\sigma}} = \boldsymbol{\sigma}^{\mathrm{ir}} \text{ or } \boldsymbol{\sigma}.\end{cases} \tag{7}$$

The flow variables have to be related through evolution laws to the force variables. To satisfy the inequality (7) some assumptions may be added to these relations. It is convenient to introduce a dissipation potential φ from which the evolution laws are derived. By duality, a force function φ^* is automatically defined using the Legendre–Fenchel transformation,

$$\begin{array}{ll}
\text{Primal complementary laws} & \text{Dual complementary laws}\\
\hat{\boldsymbol{\sigma}} \in \partial_{\dot{\hat{\boldsymbol{\varepsilon}}}}\varphi\left(\dot{\hat{\boldsymbol{\varepsilon}}},\dot{\alpha},-\dfrac{q}{T}\right), & \dot{\hat{\boldsymbol{\varepsilon}}} \in \partial_{\hat{\boldsymbol{\sigma}}}\varphi^*\left(\hat{\boldsymbol{\sigma}},\dot{\alpha},-\dfrac{q}{T}\right),\\
A \in \partial_{\dot{\alpha}}\varphi\left(\dot{\hat{\boldsymbol{\varepsilon}}},\dot{\alpha},-\dfrac{q}{T}\right), & -A \in \partial_{\dot{\alpha}}\varphi^*\left(\hat{\boldsymbol{\sigma}},\dot{\alpha},-\dfrac{q}{T}\right),\\
\nabla T \in \partial_{(-q/T)}\varphi\left(\dot{\hat{\boldsymbol{\varepsilon}}},\dot{\alpha},-\dfrac{q}{T}\right), & -\nabla T \in \partial_{(-q/T)}\varphi^*\left(\hat{\boldsymbol{\sigma}},\dot{\alpha},-\dfrac{q}{T}\right).
\end{array} \tag{8}$$

To satisfy the Clausius–Duhem inequality, some assumptions on the dissipation potential are necessary. For simplicity, we consider now an isothermal process. The left-hand side of the inequality is reduced to,

$$\hat{\boldsymbol{\sigma}}:\dot{\hat{\boldsymbol{\varepsilon}}} + A\dot{\alpha} = \frac{\partial\varphi}{\partial\dot{\hat{\boldsymbol{\varepsilon}}}}:\dot{\hat{\boldsymbol{\varepsilon}}} + \frac{\partial\varphi}{\partial\dot{\alpha}}\dot{\alpha} = \partial\varphi(\dot{\hat{\boldsymbol{\varepsilon}}},\dot{\alpha})\cdot\left(\dot{\hat{\boldsymbol{\varepsilon}}},\dot{\alpha}\right)$$

and the primal state laws are summarised as $(\hat{\boldsymbol{\sigma}}, A) \in \partial\varphi(\dot{\hat{\boldsymbol{\varepsilon}}},\dot{\alpha})$, the potential φ being a *convex function*. With a convex analysis characterisation of the subdifferential we write

$$\forall(\boldsymbol{x},y) \quad \varphi(\dot{\hat{\boldsymbol{\varepsilon}}},\dot{\alpha}) - \varphi(\boldsymbol{x},y) \leqslant \left((\dot{\hat{\boldsymbol{\varepsilon}}},\dot{\alpha}) - (\boldsymbol{x},y)\right)\cdot(\hat{\boldsymbol{\sigma}},A).$$

Table 1
Strain versus stress formulations

State variable: $\boldsymbol{\varepsilon}^{\mathrm{r}}$ $\boldsymbol{\sigma} : \dot{\boldsymbol{\varepsilon}}^{\mathrm{ir}} + A_m\dot{\alpha}_m - \frac{q}{T}\nabla T \geqslant 0$		State variable: $\boldsymbol{\sigma}$ $\dot{\boldsymbol{\varepsilon}}^{\mathrm{ir}} : \boldsymbol{\sigma} + A_m\dot{\alpha}_m - \frac{q}{T}\nabla T \geqslant 0$	
Free energy: ψ	Dissipation potential: φ	Free enthalpy: ψ^*	Force function: φ^*
$\frac{1}{\rho}\boldsymbol{\sigma} \in \partial_{\boldsymbol{\varepsilon}^{\mathrm{r}}}\psi$	$\boldsymbol{\sigma} \in \partial_{\dot{\boldsymbol{\varepsilon}}^{\mathrm{ir}}}\varphi$	$\frac{1}{\rho}\boldsymbol{\varepsilon}^{\mathrm{r}} \in \partial_{\boldsymbol{\sigma}}\psi^*$	$\dot{\boldsymbol{\varepsilon}}^{\mathrm{ir}} \in \partial_{\boldsymbol{\sigma}}\varphi^*$
$-s \in \partial_T\psi$	$A_m \in \partial_{\dot{\alpha}_m}\varphi$	$s \in \partial_T\psi^*$	$-A_m \in \partial_{\dot{\alpha}_m}\varphi^*$
$-\frac{1}{\rho}A_m \in \partial_{\alpha_m}\psi$	$\nabla T \in \partial_{(-q/T)}\varphi$	$\frac{1}{\rho}A_m \in \partial_{\alpha_m}\psi^*$	$-\nabla T \in \partial_{(-q/T)}\varphi^*$
State variable: $\boldsymbol{\varepsilon}$ $\boldsymbol{\sigma}^{\mathrm{ir}} : \dot{\boldsymbol{\varepsilon}} + A_m\dot{\alpha}_m - \frac{q}{T}\nabla T \geqslant 0$		State variable: $\boldsymbol{\sigma}^{\mathrm{r}}$ $\dot{\boldsymbol{\varepsilon}} : \boldsymbol{\sigma}^{\mathrm{ir}} + A_m\dot{\alpha}_m - \frac{q}{T}\nabla T \geqslant 0$	
Free energy: ψ	Dissipation potential: φ	Free enthalpy: ψ^*	Force function: φ^*
$\frac{1}{\rho}\boldsymbol{\sigma}^{\mathrm{r}} \in \partial_{\boldsymbol{\varepsilon}}\psi$	$\boldsymbol{\sigma}^{\mathrm{ir}} \in \partial_{\dot{\boldsymbol{\varepsilon}}}\varphi$	$\frac{1}{\rho}\boldsymbol{\varepsilon} \in \partial_{\boldsymbol{\sigma}^{\mathrm{r}}}\psi^*$	$\dot{\boldsymbol{\varepsilon}} \in \partial_{\boldsymbol{\sigma}^{\mathrm{ir}}}\varphi^*$
$-s \in \partial_T\psi$	$A_m \in \partial_{\dot{\alpha}_m}\varphi$	$s \in \partial_T\psi^*$	$-A_m \in \partial_{\dot{\alpha}_m}\varphi^*$
$-\frac{1}{\rho}A_m \in \partial_{\alpha_m}\psi$	$\nabla T \in \partial_{(-q/T)}\varphi$	$\frac{1}{\rho}A_m \in \partial_{\alpha_m}\psi^*$	$-\nabla T \in \partial_{(-q/T)}\varphi^*$

Moreover, if φ *is minimum in* $(\mathbf{0}, 0)$, the Clausius–Duhem inequality is then satisfied (Suquet, 1982),

$$\hat{\boldsymbol{\sigma}} : \dot{\hat{\boldsymbol{\varepsilon}}} + A\dot{\alpha} \geqslant \varphi(\dot{\hat{\boldsymbol{\varepsilon}}}, \dot{\alpha}) - \varphi(\mathbf{0}, 0) \geqslant 0.$$

Similar properties are required for φ^* to recover the Clausius–Duhem inequality. Generally, we distinguish the reversible and irreversible parts of the transformation. We thus postulate an additive decomposition for both reversible and irreversible parts of the strain tensor $\boldsymbol{\varepsilon} = \boldsymbol{\varepsilon}^{\mathrm{r}} + \boldsymbol{\varepsilon}^{\mathrm{ir}}$ (which is classical for the so called small strain assumption) and the stress tensor $\boldsymbol{\sigma} = \boldsymbol{\sigma}^{\mathrm{r}} + \boldsymbol{\sigma}^{\mathrm{ir}}$. The reversible/irreversible splitting of $\boldsymbol{\sigma}$ is less classical. To illustrate its interest, remark that possible residual stresses may be accounted for in the irreversible part.

At this stage, we have to choose the external state variable $\boldsymbol{X}$ for the strain formulation and consequently $\boldsymbol{X}^*$ for the stress formulation. It is usual to consider for $\boldsymbol{X}$ the total strain tensor $\boldsymbol{\varepsilon}$. By the way, the reversible stress $\boldsymbol{\sigma}^{\mathrm{r}}$ appears in the state law and becomes the state variable in the dual stress formulation. But we can also use the reversible strain part $\boldsymbol{\varepsilon}^{\mathrm{r}}$ and deduce the full stress tensor $\boldsymbol{\sigma}$ as the dual state variable (cf. Table 1). The first column expresses the primal model using $\boldsymbol{\varepsilon}^{\mathrm{r}}$ or $\boldsymbol{\varepsilon}$ as state variable. The second column provides the corresponding dual formulations.

2.2. 1D model of reinforced geomaterial

Let us apply previous results to a rheological 1D model of *TexSol* taking into account the wire unilaterality.

2.2.1. Strain formulation

We choose to superpose a classical 1D model of elasto-plasticity with hardening for sand (Lemaitre and Chaboche, 1990) and a 1D unilateral model of elasticity for wire. We thus propose the two potentials ψ (free energy) and φ (dissipation potential) depending on the external state variable ε and on the internal variable ε_2 as shown in Fig. 5,

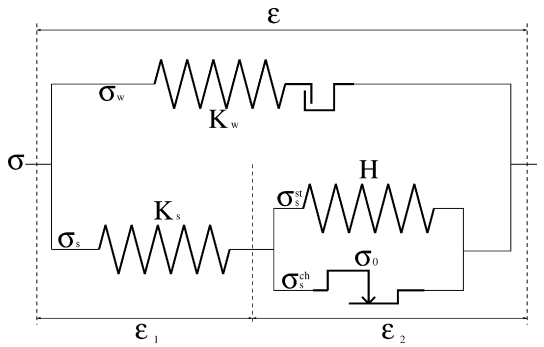

Fig. 5. Rheological *TexSol* diagram.

$$\psi(\varepsilon,\varepsilon_2)=\begin{cases}\psi_1(\varepsilon,\varepsilon_2) & \text{if } \varepsilon\in C_1,\\ \psi_2(\varepsilon,\varepsilon_2) & \text{if } \varepsilon\in C_2,\end{cases} \tag{9}$$

$$\varphi(\dot\varepsilon,\dot\varepsilon_2)=\sigma_0|\dot\varepsilon_2|, \tag{10}$$

where

$$\psi_1(\varepsilon,\varepsilon_2)=\frac{1}{2}K_w\varepsilon^2+\frac{1}{2}K_s(\varepsilon-\varepsilon_2)^2+\frac{1}{2}H{\varepsilon_2}^2,\qquad C_1=\{\varepsilon\in\mathbb{R}\mid\varepsilon\geqslant 0\},$$

$$\psi_2(\varepsilon,\varepsilon_2)=\frac{1}{2}K_s(\varepsilon-\varepsilon_2)^2+\frac{1}{2}H{\varepsilon_2}^2,\qquad C_2=\{\varepsilon\in\mathbb{R}\mid\varepsilon\leqslant 0\}$$

and σ_0 the stress threshold. According to Table 1 the state and complementary laws are derived,

State laws:

$$\sigma^{\mathrm{r}}=\frac{\partial\psi}{\partial\varepsilon}=K_w\langle\varepsilon\rangle+K_s(\varepsilon-\varepsilon_2),\qquad A=-\frac{\partial\psi}{\partial\varepsilon_2}=K_s(\varepsilon-\varepsilon_2)-H\varepsilon_2.$$

Complementary laws:

$$\sigma^{\mathrm{ir}}=\frac{\partial\varphi}{\partial\dot\varepsilon}=0,\qquad A\in\partial_{\dot\varepsilon_2}\varphi=\begin{cases}\{\operatorname{sign}\dot\varepsilon_2\sigma_0\} & \text{if } \dot\varepsilon_2\in\mathbb{R}^*,\\ [-\sigma_0,\sigma_0] & \text{if } \dot\varepsilon_2=0,\end{cases}$$

where $\langle\varepsilon\rangle=\max(0,\varepsilon)$ is the non-negative part of $\boldsymbol{\varepsilon}$ and $\operatorname{sign}(\cdot)$ is the signum operator.

2.2.2. Stress formulation

To determine the stress formulation, we have to calculate the Legendre–Fenchel transformations of ψ and φ which are not always analytically accessible. However, we can use the following general result convenient for piecewise smooth functions.

Proposition 1. *Consider a non-overlapping splitting $(C_i)_{i=1,n}$ of the strain space $\mathbb{R}^{3\times3}$, $\bigcup_{i=1}^n C_i=\mathbb{R}^{3\times3}$, C_i close convex cone with $\operatorname{mes}(C_i\cap C_j)=0$, $i\neq j$. If $\psi(\boldsymbol{\varepsilon})$ is piecewise defined by $\psi(\boldsymbol{\varepsilon})=\psi_i(\boldsymbol{\varepsilon})$ if $\boldsymbol{\varepsilon}\in C_i$, $i=1,\dots,n$, then*

$$\psi^*(\boldsymbol{\sigma})=\sup_i\big\{(\psi_i^*\nabla\mathrm{I}_{C_i^\circ})(\boldsymbol{\sigma})\big\}.$$

Proof. Let us recall the definition of inf-convolution of two functions f and g (Moreau, 1966), the indicator function of a convex set A and the polar cone C° of C,

$$\circ\ (f\nabla g)(\varepsilon)=\inf_{\varepsilon=\varepsilon_1+\varepsilon_2}\big\{f(\varepsilon_1)+f(\varepsilon_2)\big\},$$

$$\circ\ \mathrm{I}_A(\varepsilon)=\begin{cases}0 & \text{if } \varepsilon\in A,\\ +\infty & \text{if } \varepsilon\notin A,\end{cases}$$

$$\circ\ C^\circ=\big\{\boldsymbol{\sigma}\mid\boldsymbol{\varepsilon}:\boldsymbol{\sigma}\leqslant 0,\forall\boldsymbol{\varepsilon}\in C\big\}.$$

According to classical rules of convex analysis,

$$\begin{aligned}\psi^*(\boldsymbol{\sigma})&=\sup_{\bar{\boldsymbol{\varepsilon}}}\Big\{\boldsymbol{\sigma}:\bar{\boldsymbol{\varepsilon}}-\inf_i\big\{\psi_i(\bar{\boldsymbol{\varepsilon}})+\mathrm{I}_{C_i}(\bar{\boldsymbol{\varepsilon}})\big\}\Big\}=\sup_i\Big\{\sup_{\bar{\boldsymbol{\varepsilon}}}\big\{\boldsymbol{\sigma}:\bar{\boldsymbol{\varepsilon}}-\psi_i(\bar{\boldsymbol{\varepsilon}})-\mathrm{I}_{C_i}(\bar{\boldsymbol{\varepsilon}})\big\}\Big\}\\ &=\sup_i\big\{(\psi_i+\mathrm{I}_{C_i})^*(\boldsymbol{\sigma})\big\}=\sup_i\big\{(\psi_i^*\nabla\mathrm{I}_{C_i^\circ})(\boldsymbol{\sigma})\big\}.\end{aligned}$$

For the 1D model the split into two half spaces is obvious and the analytical forms of conjugate functions from (9) are accessible,

$$\psi_1^*(\sigma^{\mathrm{r}},\varepsilon_2)=\frac{(\sigma^{\mathrm{r}}+K_s\varepsilon_2)^2}{2(K_w+K_s)}-\frac{(K_s+H){\varepsilon_2}^2}{2},\quad C_1^\circ=\{\sigma\in\mathbb{R}\mid\sigma\leqslant 0\},$$

$$\psi_2^*(\sigma^{\mathrm{r}},\varepsilon_2)=\frac{(\sigma^{\mathrm{r}}+K_s\varepsilon_2)^2}{2K_s}-\frac{(K_s+H){\varepsilon_2}^2}{2},\quad C_2^\circ=\{\sigma\in\mathbb{R}\mid\sigma\geqslant 0\}.$$

Using Proposition 1, we obtain successively,

$$\psi_1^*\nabla \mathrm{I}_{C_1^\circ} = \begin{cases} -\dfrac{(K_s+H){\varepsilon_2}^2}{2} & \text{if } \sigma^{\mathrm{r}} + K_s\varepsilon_2 \leqslant 0, \\ \dfrac{(\sigma^{\mathrm{r}} + K_s\varepsilon_2)^2}{2(K_w+K_s)} - \dfrac{(K_s+H){\varepsilon_2}^2}{2} & \text{if } \sigma^{\mathrm{r}} + K_s\varepsilon_2 \geqslant 0, \end{cases}$$

$$\psi_2^*\nabla \mathrm{I}_{C_2^\circ} = \begin{cases} -\dfrac{(K_s+H){\varepsilon_2}^2}{2} & \text{if } \sigma^{\mathrm{r}} + K_s\varepsilon_2 \geqslant 0, \\ \dfrac{(\sigma^{\mathrm{r}} + K_s\varepsilon_2)^2}{2K_s} - \dfrac{(K_s+H){\varepsilon_2}^2}{2} & \text{if } \sigma^{\mathrm{r}} + K_s\varepsilon_2 \leqslant 0. \end{cases}$$

Finally,

$$\psi^*\big(\sigma^{\mathrm{r}}, \varepsilon_2\big) = \begin{cases} \dfrac{(\sigma^{\mathrm{r}} + K_s\varepsilon_2)^2}{2(K_w+K_s)} - \dfrac{(K_s+H){\varepsilon_2}^2}{2} & \text{if } \sigma^{\mathrm{r}} + K_s\varepsilon_2 \geqslant 0, \\ \dfrac{(\sigma^{\mathrm{r}} + K_s\varepsilon_2)^2}{2K_s} - \dfrac{(K_s+H){\varepsilon_2}^2}{2} & \text{if } \sigma^{\mathrm{r}} + K_s\varepsilon_2 \leqslant 0. \end{cases} \tag{11}$$

The Legendre–Fenchel transformation of the dissipation potential is computed classically from (10),

$$\varphi^*\big(\sigma^{\mathrm{ir}}, \dot{\varepsilon}_2\big) = \mathrm{I}_{\{0\}}\big(\sigma^{\mathrm{ir}}\big) - \sigma_0|\dot{\varepsilon}_2|. \tag{12}$$

From Eq. (12) we implicitly get $\sigma^{\mathrm{ir}} = 0$. The state and complementary laws in the stress formulation are derived in a straightforward manner.

State laws:

$$\varepsilon = \frac{\partial \psi^*}{\partial \sigma^{\mathrm{r}}}\big(\sigma^{\mathrm{ir}}, \varepsilon_2\big) = \begin{cases} \dfrac{\sigma^{\mathrm{r}} + K_s\varepsilon_2}{K_w+K_s} & \text{if } \sigma^{\mathrm{r}} + K_s\varepsilon_2 \geqslant 0, \\ \dfrac{\sigma^{\mathrm{r}} + K_s\varepsilon_2}{K_s} & \text{if } \sigma^{\mathrm{r}} + K_s\varepsilon_2 \leqslant 0, \end{cases}$$

$$A = \frac{\partial \psi^*}{\partial \varepsilon_2}\big(\sigma^{\mathrm{ir}}, \varepsilon_2\big) = \begin{cases} \dfrac{K_s}{K_w+K_s}(\sigma^{\mathrm{r}} + K_s\varepsilon_2) - (K_s+H)\varepsilon_2 & \text{if } \sigma^{\mathrm{r}} + K_s\varepsilon_2 \geqslant 0, \\ \sigma^{\mathrm{r}} + K_s\varepsilon_2 - (K_s+H)\varepsilon_2 & \text{if } \sigma^{\mathrm{r}} + K_s\varepsilon_2 \leqslant 0. \end{cases}$$

Complementary laws:

$$\dot{\varepsilon} \in \partial_{\sigma^{\mathrm{ir}}}\varphi^*\big(\sigma^{\mathrm{ir}}, \dot{\varepsilon}_2\big) = \mathbb{R}$$

$$A \in -\partial_{\dot{\varepsilon}_2}\varphi^*\big(\sigma^{\mathrm{ir}}, \dot{\varepsilon}_2\big) = \begin{cases} \big\{\operatorname{sign}\dot{\varepsilon}_2\sigma_0\big\} & \text{if } \dot{\varepsilon}_2 \in \mathbb{R}^*, \\ [-\sigma_0, \sigma_0] & \text{if } \dot{\varepsilon}_2 = 0. \end{cases}$$

This set of equations is equivalent to the one obtained with the strain formulation Section 2.2.1.

3. Strain and stress approach for 3D models

The three dimensional effects cannot be neglected in modelling the complex microstructure of the *TexSol* material. To define a 3D model, we follow the previous 1D approach superposing a classical elastic plastic behaviour for the sand and a unilateral elastic one for the wire network. Simple and sophisticated unilaterality conditions may be considered leading to different formulations more or less easy to handle in a general primal/dual framework.

3.1. 3D thermodynamical potentials of the sand

First of all, let us recall that the stress tensor can be split into a spherical part and a deviatoric one,

$$\boldsymbol{\sigma} = \underbrace{\frac{1}{3}\operatorname{tr}(\boldsymbol{\sigma})\boldsymbol{I}}_{\text{spherical}} + \underbrace{\boldsymbol{S}}_{\text{deviatoric}},$$

where $\boldsymbol{I}$ is the identity second order tensor ($I_{ij} = \delta_{ij}$) and tr$(\cdot)$ is the trace operator. Let us introduce the spherical projection tensor $\mathbb{S} = \frac{1}{3}\boldsymbol{I} \otimes \boldsymbol{I}$ and the deviatoric projection tensor $\mathbb{D} = \mathbb{I} - \mathbb{S}$ where $\mathbb{I}$ is the identity fourth order tensor ($I_{ijkl} = \frac{1}{2}(\delta_{ik}\delta_{jl} + \delta_{il}\delta_{jk})$). In a classical model the state variable is sand's full strain $\boldsymbol{\varepsilon}_s$, the internal variables contain the plastic strain $\boldsymbol{\varepsilon}_s^{\mathrm{p}}$, the kinematic and isotropic hardening variables $\boldsymbol{\alpha}$ and p (Wood, 1990). The free energy ψ_s has the following form,

$$\psi_s\big(\boldsymbol{\varepsilon}_s, \boldsymbol{\varepsilon}_s^{\mathrm{p}}, \boldsymbol{\alpha}, p\big) = \frac{1}{2}\big(\boldsymbol{\varepsilon}_s - \boldsymbol{\varepsilon}_s^{\mathrm{p}}\big) : \mathbb{K}_s\big(\boldsymbol{\varepsilon}_s - \boldsymbol{\varepsilon}_s^{\mathrm{p}}\big) + \frac{H_k}{2}\boldsymbol{\alpha} : \boldsymbol{\alpha} + \frac{H_i}{2}p^2, \tag{13}$$

where $\mathbb{K}_s$, H_k and H_i are stiffness coefficients. The state laws are directly derived from it,

$$\begin{aligned}
\boldsymbol{\sigma}_s^{\mathrm{r}} &= \frac{\partial \psi_s}{\partial \boldsymbol{\varepsilon}_s} = \mathbb{K}_s\big(\boldsymbol{\varepsilon}_s - \boldsymbol{\varepsilon}_s^{\mathrm{p}}\big),\\
\boldsymbol{A} &= -\frac{\partial \psi_s}{\partial \boldsymbol{\varepsilon}_s^{\mathrm{p}}} = \mathbb{K}_s\big(\boldsymbol{\varepsilon}_s - \boldsymbol{\varepsilon}_s^{\mathrm{p}}\big),\\
\boldsymbol{\chi} &= -\frac{\partial \psi_s}{\partial \boldsymbol{\alpha}} = -H_k\boldsymbol{\alpha},\\
R &= -\frac{\partial \psi_s}{\partial p} = -H_i\, p.
\end{aligned} \tag{14}$$

To derive the complementary laws, it is more convenient to define the force function φ^* instead of the dissipation potential φ,

$$\varphi_s^*\big(\boldsymbol{\sigma}_s^{\mathrm{ir}}, \boldsymbol{A}, \boldsymbol{\chi}, R\big) = \mathrm{I}_{\{\boldsymbol{0}\}}\big(\boldsymbol{\sigma}_s^{\mathrm{ir}}\big) + \mathrm{I}_{\Omega(\boldsymbol{\chi},R)}(\boldsymbol{A}), \tag{15}$$

where $\Omega(\boldsymbol{\chi}, R) = \{\boldsymbol{A} \mid F(\boldsymbol{A}, \boldsymbol{\chi}, R) \leqslant 0\}$ is the elastic domain bounded by the *Drucker–Prager* criterion F defined by (Drucker and Prager, 1952),

$$F(\boldsymbol{A}, \boldsymbol{\chi}, R) = \sqrt{J_2(\boldsymbol{A} - \boldsymbol{\chi})} - \tau_y(\boldsymbol{A}) - R(p). \tag{16}$$

Remark that $\sqrt{J_2(\cdot)}$ is the pseudo norm of the tensor deviatoric part implied in the plastic phenomenon (where J_2 is the second invariant). The initial threshold τ_y depends on the pressure (as it is usual in soil mechanics), on the friction coefficient β related to the friction angle θ_f ($\beta = \tan(\theta_f)$) and on the cohesion parameter C_0, $\tau_y(\boldsymbol{A}) = C_0 - \beta\,\mathrm{tr}(\boldsymbol{A}) = \sigma_y/\sqrt{3}$. The Drucker–Prager yield criterion is smooth on its deviatoric part and it depends only on two invariants $J_1 = \mathrm{tr}(\cdot)$ and J_2. Moreover, for friction angles below 30° (Desrues, 2002), it gives a good approximation of the Mohr–Coulomb yield criterion which is classically used for sand. Other models can be used to define the soil plasticity such as those proposed by Vermeer and Nova. Since we use the dual dissipation potential, we get the complementary laws usually obtained from the stress formulation (cf. Table 1),

$$\begin{aligned}
\dot{\boldsymbol{\varepsilon}} &\in \partial_{\boldsymbol{\sigma}_s^{\mathrm{ir}}}\varphi^*\big(\boldsymbol{\sigma}_s^{\mathrm{ir}}, \boldsymbol{A}, \boldsymbol{\chi}, R\big) = \mathbb{R}^{3\times 3},\\
\dot{\boldsymbol{\varepsilon}}_s^{\mathrm{p}} &= \dot{\lambda}\frac{\partial F}{\partial \boldsymbol{A}}(\boldsymbol{A}, \boldsymbol{\chi}, R) = \dot{\lambda}\left[\frac{\boldsymbol{A} - \boldsymbol{\chi}}{2\sqrt{J_2(\boldsymbol{A} - \boldsymbol{\chi})}} + \beta\boldsymbol{I}\right],\\
\dot{\boldsymbol{\alpha}} &= \dot{\lambda}\frac{\partial F}{\partial \boldsymbol{\chi}}(\boldsymbol{A}, \boldsymbol{\chi}, R) = -\dot{\lambda}\frac{\boldsymbol{A} - \boldsymbol{\chi}}{2\sqrt{J_2(\boldsymbol{A} - \boldsymbol{\chi})}},\\
\dot{p} &= \dot{\lambda}\frac{\partial F}{\partial R}(\boldsymbol{A}, \boldsymbol{\chi}, R) = -\dot{\lambda},
\end{aligned} \tag{17}$$

where $\dot{\lambda}$ is the plastic multiplier always non-negative. Its value can be found with the plastic condition $F = 0$ and the consistency condition $\dot{F} = 0$,

$$\begin{cases} F = 0 \\ \dot{F} = 0 \end{cases} \quad \Rightarrow \quad \begin{cases} \sqrt{J_2(\boldsymbol{A} - \boldsymbol{\chi})} = \tau_y(\boldsymbol{A}) + R(p), \\ \dot{\lambda} = \dfrac{1}{H_i + H_k/2}\left(\dfrac{\boldsymbol{A} - \boldsymbol{\chi}}{2(\tau_y(\boldsymbol{A}) + R(p))} + \beta\boldsymbol{I}\right) : \dot{\boldsymbol{A}}. \end{cases} \tag{18}$$

In contrast to the 1D case, we cannot explicitly express a 3D dissipation potential depending on flow variables.

3.2. Unilateral wire network model

According to the 1D model, we neglect the dissipation effects, and we focus on the free energy. Its stiffness cannot be reduced to the stiffness of the wire and has to account for the wire distribution in the sample, assumed to be isotropic in the following. Due to the entanglement of the wire network, it is convenient to consider continuously differentiable free energy to derive smooth relations between strain and stress at the macroscopic level. A model directly derived from the isotropic linear elasticity may be expressed in the principal directions; the strain and stress tensors assumed to be coaxial. This property is lost when the unilaterality is considered and we can derive two different models starting either from a strain approach or a stress approach. For instance, using the Lamé coefficients λ_w, μ_w and the strain principal values denoted ε_w^1, ε_w^2, ε_w^3 (we introduce the notations $\tilde{\boldsymbol{\varepsilon}}_w = \operatorname{diag}(\varepsilon_w^1, \varepsilon_w^2, \varepsilon_w^3)$ and $\langle\tilde{\boldsymbol{\varepsilon}}_w\rangle = \operatorname{diag}(\langle\varepsilon_w^1\rangle, \langle\varepsilon_w^2\rangle, \langle\varepsilon_w^3\rangle)$, where $\operatorname{diag}(a, b, c)$ is a diagonal matrix with the diagonal coefficients a, b and c) the free energy may be defined by,

$$\psi_w(\boldsymbol{\varepsilon}_w) = \frac{\lambda_w}{2}\big\langle\varepsilon_w^1 + \varepsilon_w^2 + \varepsilon_w^3\big\rangle^2 + \mu_w\big(\big\langle\varepsilon_w^1\big\rangle^2 + \big\langle\varepsilon_w^2\big\rangle^2 + \big\langle\varepsilon_w^3\big\rangle^2\big). \tag{19}$$

The first term describes the bulk unilateral behaviour of the wire network activated by the trace of the strain. The second part concerns the shear component which is not activated in all directions simultaneously but according to the sign of the strain principal values. With a stress approach we could formulate a similar expression for the free enthalpy but using the principal values of the wire stress tensor.

$$\mathcal{G}_w(\boldsymbol{\sigma}_w) = \frac{1-2\nu_w}{6E_w}\big\langle\sigma_w^1 + \sigma_w^2 + \sigma_w^3\big\rangle^2 + \frac{1+\nu_w}{2E_w}\big(\big\langle S_w^1\big\rangle^2 + \big\langle S_w^2\big\rangle^2 + \big\langle S_w^3\big\rangle^2\big), \tag{20}$$

where $\boldsymbol{S}_w$ is the deviatoric part of $\boldsymbol{\sigma}_w$. The stress expressed in the principal directions is easily derived from (19),

$$\tilde{\boldsymbol{\sigma}}_w^{\mathrm{r}} = \frac{\mathrm{d}\psi_w}{\mathrm{d}\tilde{\boldsymbol{\varepsilon}}_w}(\tilde{\boldsymbol{\varepsilon}}_w) = \lambda_w\big\langle\operatorname{tr}(\tilde{\boldsymbol{\varepsilon}}_w)\big\rangle\boldsymbol{I} + 2\mu_w\big\langle\tilde{\boldsymbol{\varepsilon}}_w\big\rangle.$$

In the current frame, the strain-stress relationship has the form,

$$\boldsymbol{\sigma}_w^{\mathrm{r}} = \lambda_w\big\langle\operatorname{tr}(\boldsymbol{\varepsilon}_w)\big\rangle\boldsymbol{I} + 2\mu_w\boldsymbol{P}\big\langle\tilde{\boldsymbol{\varepsilon}}_w\big\rangle\boldsymbol{P}^{\mathrm{T}}, \tag{21}$$

where $\boldsymbol{P}$ depending on $\boldsymbol{\varepsilon}_w$ is the transformation matrix from the principal directions to the current ones. The expression $\boldsymbol{P}\langle\tilde{\boldsymbol{\varepsilon}}_w\rangle\boldsymbol{P}^{\mathrm{T}}$ is the positive part of the wire strain tensor denoted $\boldsymbol{\varepsilon}_w^{\geqslant}$. The convexity of the free energy is easily satisfied for $\mu_w = 0$ because the trace is a linear operator. When $\mu_w \neq 0$, the convexity is proved using a composition argument given in (Yang, 1980).

In (De Buhan and Sudret, 1999) a two-phase elastoplastic model for unidirectionally reinforced material is proposed, i.e., the reinforcement network takes the form of a uniaxial stress variable. In our approach, we consider a three-dimensional reinforcement coupled with a strong unilateral condition. We use the same assumption of equality strain rates (Section 1.2) to superpose both sand and wire models.

3.3. Models superposition and TexSol potentials

The previous models are combined according to the 1D approach. Moreover, we introduce two possible initial stresses $\boldsymbol{\sigma}_w^0$ and $\boldsymbol{\sigma}_s^0$. These are generated by the deposit process under gravity which may be simulated by a discrete element software (Dubois and Jean, 2003; Moreau, 1999). Then we can reasonably assume that principal values of $\boldsymbol{\sigma}_w^0$ are non-negatives. We define the corresponding initial strains using the elastic parts of the previous models, $\boldsymbol{\varepsilon}_w^0 = \mathbb{K}_w^{-1}\boldsymbol{\sigma}_w^0$ and $\boldsymbol{\varepsilon}_s^0 = \mathbb{K}_s^{-1}\boldsymbol{\sigma}_s^0$, where $\mathbb{K}_w = \lambda_w\boldsymbol{I}\otimes\boldsymbol{I} + 2\mu_w\mathbb{I}$. The total free energy is then postulated,

$$\begin{aligned}\psi\big(\boldsymbol{\varepsilon}, \boldsymbol{\varepsilon}^{\mathrm{p}}, \boldsymbol{\alpha}, p\big) = {}& \frac{1}{2}\big(\boldsymbol{\varepsilon} - \boldsymbol{\varepsilon}^{\mathrm{p}} + \boldsymbol{\varepsilon}_s^0\big) : \mathbb{K}_s\big(\boldsymbol{\varepsilon} - \boldsymbol{\varepsilon}^{\mathrm{p}} + \boldsymbol{\varepsilon}_s^0\big) + \frac{\lambda_w}{2}\big\langle\operatorname{tr}\big(\boldsymbol{\varepsilon} + \boldsymbol{\varepsilon}_w^0\big)\big\rangle^2 + \mu_w\big(\boldsymbol{\varepsilon} + \boldsymbol{\varepsilon}_w^0\big)^{\geqslant} : \big(\boldsymbol{\varepsilon} + \boldsymbol{\varepsilon}_w^0\big)^{\geqslant} \\ & + \frac{H_k}{2}\boldsymbol{\alpha} : \boldsymbol{\alpha} + \frac{H_i}{2}p^2.\end{aligned} \tag{22}$$

The state laws are derived,

$$\boldsymbol{\sigma}^{\mathrm{r}} = \frac{\partial \psi}{\partial \boldsymbol{\varepsilon}} = \mathbb{K}_s\big(\boldsymbol{\varepsilon} - \boldsymbol{\varepsilon}^{\mathrm{p}}\big) + \boldsymbol{\sigma}_s^0 + \lambda_w\big\langle \mathrm{tr}\big(\boldsymbol{\varepsilon} + \boldsymbol{\varepsilon}_w^0\big)\big\rangle \boldsymbol{I} + 2\mu_w\big(\boldsymbol{\varepsilon} + \boldsymbol{\varepsilon}_w^0\big)^{\geqslant},$$

$$\boldsymbol{A} = -\frac{\partial \psi}{\partial \boldsymbol{\varepsilon}^{\mathrm{p}}} = \mathbb{K}_s\big(\boldsymbol{\varepsilon} - \boldsymbol{\varepsilon}^{\mathrm{p}}\big) + \boldsymbol{\sigma}_s^0,$$

$$\boldsymbol{\chi} = -\frac{\partial \psi}{\partial \boldsymbol{\alpha}} = -H_k \boldsymbol{\alpha},$$

$$R = -\frac{\partial \psi}{\partial p} = -H_i\, p. \tag{23}$$

The complementary laws are derived considering the dual dissipation potential of the sand alone (cf. Eq. (15)). In the simple case where $\mu_w = 0$, we can complete the dual stress formulation by computing the Legendre–Fenchel transformation of the free energy ψ (denoted in this case $\psi_\circ$) via the Proposition 1.

$$\psi_\circ^*\big(\boldsymbol{\sigma}^{\mathrm{r}}, \boldsymbol{\varepsilon}^{\mathrm{p}}, \boldsymbol{\alpha}, p\big) = \begin{cases} \dfrac{1}{2}\big(\boldsymbol{\sigma}^{\mathrm{r}} + \mathbb{K}_s\big(\boldsymbol{\varepsilon}^{\mathrm{p}} - \boldsymbol{\varepsilon}_s^0\big) + \boldsymbol{\sigma}_w^0\big) : \big(\mathbb{K}_s + \mathbb{K}_w^\circ\big)^{-1}\big(\boldsymbol{\sigma}^{\mathrm{r}} + \mathbb{K}_s\big(\boldsymbol{\varepsilon}^{\mathrm{p}} - \boldsymbol{\varepsilon}_s^0\big) + \boldsymbol{\sigma}_w^0\big) \\ \quad -\dfrac{1}{2}\big(\big(\boldsymbol{\varepsilon}^{\mathrm{p}} - \boldsymbol{\varepsilon}_s^0\big) : \mathbb{K}_s\big(\boldsymbol{\varepsilon}^{\mathrm{p}} - \boldsymbol{\varepsilon}_s^0\big) + H_k \boldsymbol{\alpha} : \boldsymbol{\alpha} + H_i\, p^2\big) - \dfrac{1}{2}\boldsymbol{\varepsilon}_w^0 : \boldsymbol{\sigma}_w^0 \\ \quad \text{if } \mathrm{tr}\big(\boldsymbol{\sigma}^{\mathrm{r}} + \mathbb{K}_s\big(\boldsymbol{\varepsilon}^{\mathrm{p}} - \boldsymbol{\varepsilon}_s^0 - \boldsymbol{\varepsilon}_w^0\big)\big) \geqslant 0, \\ \dfrac{1}{2}\big(\boldsymbol{\sigma}^{\mathrm{r}} + \mathbb{K}_s\big(\boldsymbol{\varepsilon}^{\mathrm{p}} - \boldsymbol{\varepsilon}_s^0\big)\big) : \mathbb{K}_s^{-1}\big(\boldsymbol{\sigma}^{\mathrm{r}} + \mathbb{K}_s\big(\boldsymbol{\varepsilon}^{\mathrm{p}} - \boldsymbol{\varepsilon}_s^0\big)\big) \\ \quad -\dfrac{1}{2}\big(\big(\boldsymbol{\varepsilon}^{\mathrm{p}} - \boldsymbol{\varepsilon}_s^0\big) : \mathbb{K}_s\big(\boldsymbol{\varepsilon}^{\mathrm{p}} - \boldsymbol{\varepsilon}_s^0\big) + H_k \boldsymbol{\alpha} : \boldsymbol{\alpha} + H_i\, p^2\big) \\ \quad \text{if } \mathrm{tr}\big(\boldsymbol{\sigma}^{\mathrm{r}} + \mathbb{K}_s\big(\boldsymbol{\varepsilon}^{\mathrm{p}} - \boldsymbol{\varepsilon}_s^0 - \boldsymbol{\varepsilon}_w^0\big)\big) \leqslant 0, \end{cases} \tag{24}$$

where $\mathbb{K}_w^\circ = \lambda_w \boldsymbol{I} \otimes \boldsymbol{I}$. In this expression it is difficult to distinguish a contribution of the unilaterality of the wire network as given in (20). Consequently the two approaches (19) and (20) are no more equivalent when unilaterality occurs (Lucchesi et al., 2000). The Legendre–Fenchel transformation cannot be catched in the more general case.

4. Numerical development

Starting from a consistent thermodynamic model for the *TexSol*, the next step consists in implementing it in a finite element software (Keryvin, 1999; Kichenin and Charras, 2003). We discuss then responses provided by the simulation of simple compression/traction tests according to the expected behaviours detailed in Section 1.

4.1. Numerical implementation

The variables being known at step $n-1$, we have to compute them at step n using a predicted value of the strain increment $\Delta\boldsymbol{\varepsilon}_n$. For the sake of simplicity, the initial stresses are neglected ($\boldsymbol{\sigma}_s^0 = \boldsymbol{\sigma}_w^0 = \boldsymbol{0}$). Two sets of variables, $(\boldsymbol{\sigma}_{s,n}, \boldsymbol{\chi}_n, p_n)$ for the sand and $(\boldsymbol{\sigma}_{w,n})$ for wire network are computed simultaneously. The stress in the wire network is directly deduced from the potential defined by (19). For sand, the relations given in (14), (17) and (18) can be reduced to three equations depending on the three unknowns $(\boldsymbol{\sigma}_{s,n}, \boldsymbol{\chi}_n, p_n)$. This system is solved by the Newton–Raphson method applied to the following residuals $\boldsymbol{Q}_n^\alpha; \alpha = 1, 2, 3$.

$$\boldsymbol{Q}_n^1 = \frac{p_n - p_{n-1}}{2(R_n + \tau_{y,n})}\big(\boldsymbol{S}_{s,n} - \boldsymbol{\chi}_n + 2(R_n + \tau_{y,n})\beta \boldsymbol{I}\big) + \Delta\boldsymbol{\varepsilon}_n - {\mathbb{K}_s}^{-1}(\boldsymbol{\sigma}_{s,n} - \boldsymbol{\sigma}_{s,n-1}),$$

$$\boldsymbol{Q}_n^2 = \frac{H_k(p_n - p_{n-1})}{2(R_n + \tau_{y,n})}(\boldsymbol{S}_{s,n} - \boldsymbol{\chi}_n) + \boldsymbol{\chi}_n - \boldsymbol{\chi}_{n-1},$$

$$Q_n^3 = \frac{1}{(R_n + \tau_{y,n})(H_k + 2H_i)}\big(\boldsymbol{S}_{s,n} - \boldsymbol{\chi}_n + 2(R_n + \tau_{y,n})\beta \boldsymbol{I}\big) : (\boldsymbol{\sigma}_{s,n} - \boldsymbol{\sigma}_{s,n-1}) + p_n - p_{n-1},$$

where $\alpha = 1$ corresponds to Eqs. (2), $(14)_1$, $(17)_{2,4}$ and $(18)_1$, $\alpha = 2$ corresponds to Eqs. $(14)_3$, $(17)_{3,4}$ and $(18)_1$ and finally $\alpha = 3$ corresponds to Eqs. $(17)_4$ and $(18)_{1,2}$ (in all these equations, R_n is calculated using Eq. $(14)_4$). Classically, the Taylor development is defined as follows

$$\boldsymbol{Q}_{n,i+1}^{\alpha} = \boldsymbol{Q}_{n,i}^{\alpha} + \left(\frac{\partial \boldsymbol{Q}_n^{\alpha}}{\partial \boldsymbol{\sigma}_{s,n}}\right)_i \delta\boldsymbol{\sigma}_{s,n,i+1} + \left(\frac{\partial \boldsymbol{Q}_n^{\alpha}}{\partial \boldsymbol{\chi}_n}\right)_i \delta\boldsymbol{\chi}_{n,i+1} + \left(\frac{\partial \boldsymbol{Q}_n^{\alpha}}{\partial p_n}\right)_i \delta p_{n,i+1}.$$

The analytical formulations of the local tangent matrix coefficients are

$$\frac{\partial \boldsymbol{Q}_n^1}{\partial \boldsymbol{\sigma}_{s,n}} = \frac{p_n - p_{n-1}}{2(R_n + \tau_{y,n})^2}\big[(R_n + \tau_{y,n})\mathbb{D} + \beta(\boldsymbol{S}_{s,n} - \boldsymbol{\chi}_n) \otimes \boldsymbol{I}\big] - {\mathbb{K}_s}^{-1},$$

$$\frac{\partial \boldsymbol{Q}_n^1}{\partial \boldsymbol{\chi}_n} = -\frac{p_n - p_{n-1}}{2(R_n + \tau_{y,n})}\mathbb{I},$$

$$\frac{\partial \boldsymbol{Q}_n^1}{\partial p_n} = \frac{R_n + \tau_{y,n} + H_i(p_n - p_{n-1})}{2(R_n + \tau_{y,n})^2}(\boldsymbol{S}_{s,n} - \boldsymbol{\chi}_n) + \beta \boldsymbol{I},$$

$$\frac{\partial \boldsymbol{Q}_n^2}{\partial \boldsymbol{\sigma}_{s,n}} = \frac{H_k(p_n - p_{n-1})}{2(R_n + \tau_{y,n})^2}\big[(R_n + \tau_{y,n})\mathbb{D} + \beta(\boldsymbol{S}_{s,n} - \boldsymbol{\chi}_n) \otimes \boldsymbol{I}\big],$$

$$\frac{\partial \boldsymbol{Q}_n^2}{\partial \boldsymbol{\chi}_n} = \left(1 - H_k \frac{p_n - p_{n-1}}{2(R_n + \tau_{y,n})}\right)\mathbb{I},$$

$$\frac{\partial \boldsymbol{Q}_n^2}{\partial p_n} = H_k \frac{R_n + \tau_{y,n} + H_i(p_n - p_{n-1})}{2(R_n + \tau_{y,n})^2}(\boldsymbol{S}_{s,n} - \boldsymbol{\chi}_n),$$

$$\frac{\partial Q_n^3}{\partial \boldsymbol{\sigma}_{s,n}} = C_n^1\big(2\boldsymbol{S}_{s,n} - \boldsymbol{S}_{s,n-1} - \boldsymbol{\chi}_n + 2(R_n + \tau_{y,n})\beta \boldsymbol{I}\big) + C_n^2(\boldsymbol{S}_{s,n} - \boldsymbol{\chi}_n) : (\boldsymbol{\sigma}_{s,n} - \boldsymbol{\sigma}_{s,n-1})\boldsymbol{I},$$

$$\frac{\partial Q_n^3}{\partial \boldsymbol{\chi}_n} = -C_n^1(\boldsymbol{\sigma}_{s,n} - \boldsymbol{\sigma}_{s,n-1}),$$

$$\frac{\partial Q_n^3}{\partial p_n} = 1 + C_n^3\big(\boldsymbol{S}_{s,n} - \boldsymbol{\chi}_n - 2(R_n + \tau_{y,n})\beta \boldsymbol{I}\big) : (\boldsymbol{\sigma}_{s,n} - \boldsymbol{\sigma}_{s,n-1}),$$

where

$$C_n^1(R_n, \tau_{y,n}) = \frac{1}{(R_n + \tau_{y,n})(H_k + 2H_i)}, \qquad C_n^2(R_n, \tau_{y,n}) = \frac{\beta C_n^1}{R_n + \tau_{y,n}}$$

and finally

$$C_n^3(R_n, \tau_{y,n}) = \frac{H_i C_n^1}{R_n + \tau_{y,n}}.$$

The algorithm is stigmatised in Table 2 (where $(\zeta_n^1, \zeta_n^2, \zeta_n^3) = (\boldsymbol{\sigma}_{s,n}, \boldsymbol{\chi}_n, p_n)$). This last one being quite complex for sand, we have compared the results given by the previous integration law and strategy with the one developed in the *Cast3M* software where a Drucker–Prager model is available. Since we got a good agreement with both implementations, we focus our attention on the coupled sand/wire model of *TexSol* involving a unilateral behaviour. A consistent tangent matrix can be used to increase the convergence rate (Simo and Hugues, 1998).

4.2. Patch test

In a first step, the simple patch test considered is a single Q1-Lagrange hexahedron finite element submitted to a traction/compression loading (cf. Fig. 6). More precisely, a confinement pressure is prescribed via a cohesion behaviour on the material (Radjaï et al., 2001) depending on a single coefficient C_0. A displacement is imposed on the upperside. Four models are compared to emphasise the relevance of the two unilateral behaviour laws. Two of them are considered to obtain some limit behaviours; the first one denoted *Sand*, is free of wire; the second one denoted

Table 2
Solution algorithm

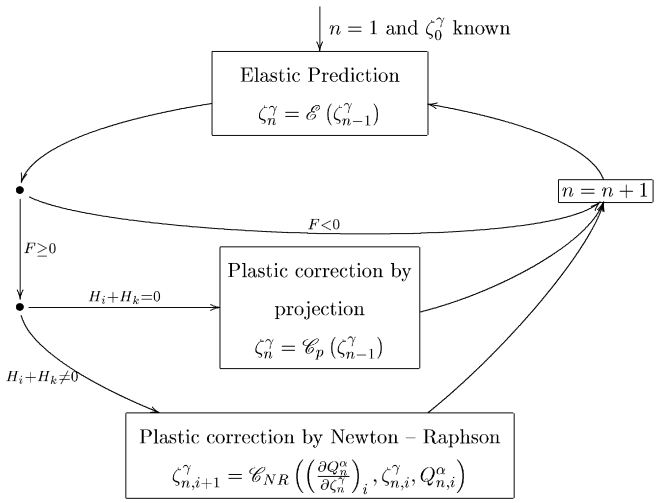

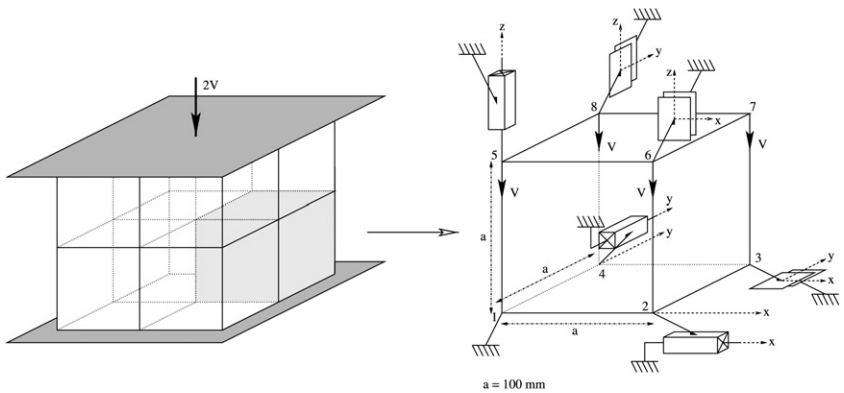

Fig. 6. Patch test.

Reinforced sand, is a superposition of a sand model and an elastic "bilateral" model of the reinforcement. The "unilateral" *TexSol* model introduced in Section 3.3 is denoted *Texsol*. A particular model is added denoted *Spherical Texsol* corresponding to the previous one with $\mu_w = 0$.

- Elasticity: $E_s = 200$ MPa, $\nu_s = 0.4$, $E_w = 100$ MPa, $\nu_w = 0.3$,
- Plasticity: $C_0 = 50$ kPa, $\theta_f = 0.1$, $H_k = 1$ MPa, $H_i = 1$ MPa.

Sand and *Reinforced sand* appear clearly as two elastic bounds for *TexSol* models (cf. Fig. 7). At this stage, *Spherical Texsol* does not differ from *Sand*. On the contrary, the *Texsol* is close to *Sand* in compression and close to *Reinforced sand* in traction. For the two loadings the limit models appear to be the upper bounds. For a loading-unloading traction process, the *Texsol* model behaves almost like *Reinforced sand* as expected (cf. Fig. 8). *Spherical Texsol* does not improve significantly *Sand* (cf. Figs. 8 and 9). Consequently, *Spherical Texsol* does not account for the numerical results given in Fig. 3 for the same kind of experiment – even roughly.

4.3. Cyclic loading

TexSol embankments may be submitted to vibrational solicitations. A cyclic test based on the test represented in Fig. 10 (where the displacements are fixed on the lower side and the solicitation controlled by force) is performed to highlight the contribution of the "unilateral" reinforcement due to the wire network. The friction angle is changed

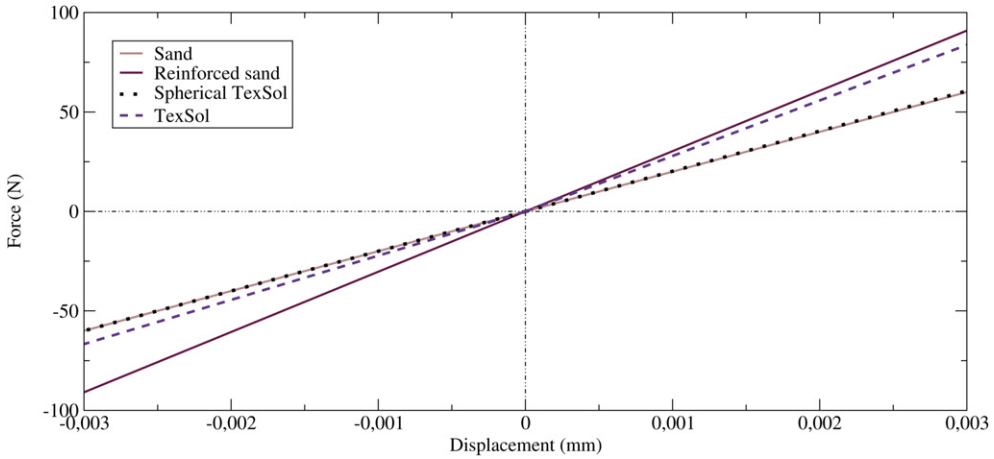

Fig. 7. Zoom on the elastic range of the models.

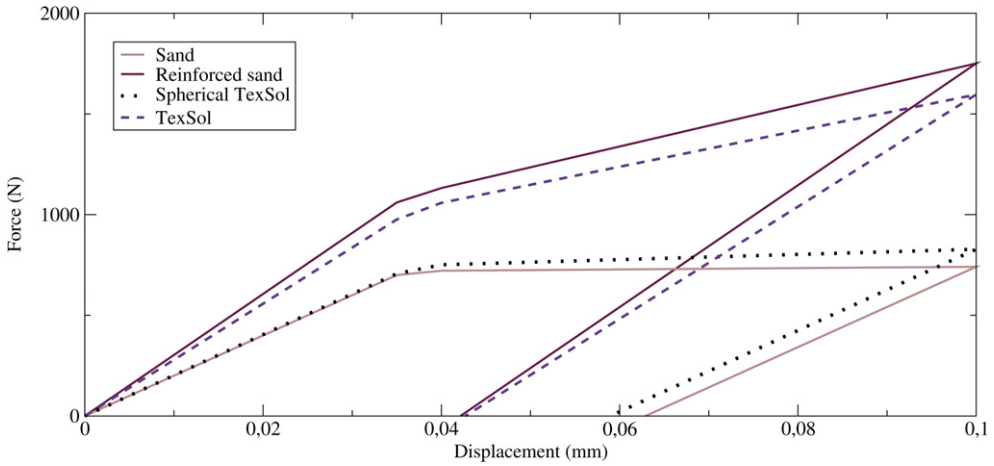

Fig. 8. Different material behaviours on a traction patch test.

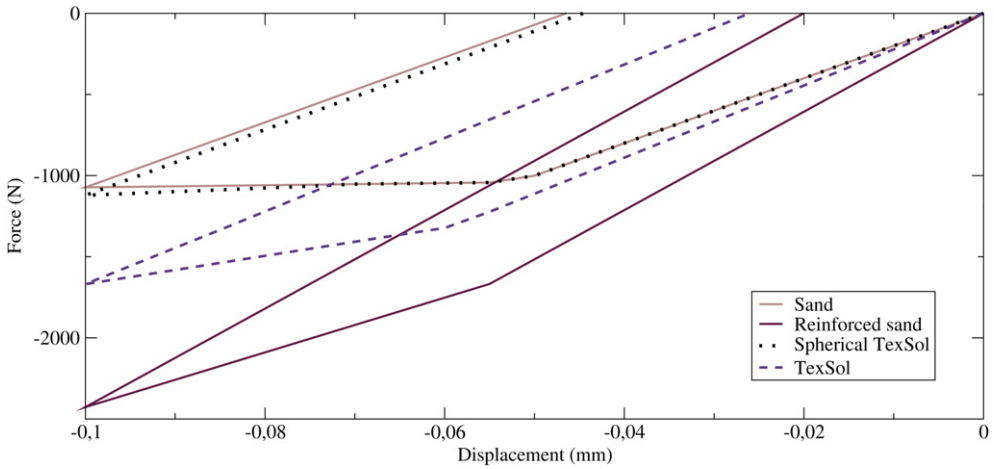

Fig. 9. Different material behaviours on a compression patch test.

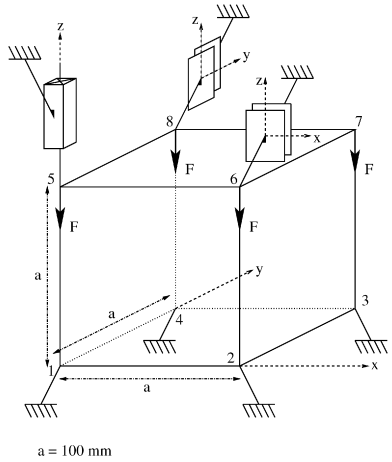

Fig. 10. Force managed traction/compression test.

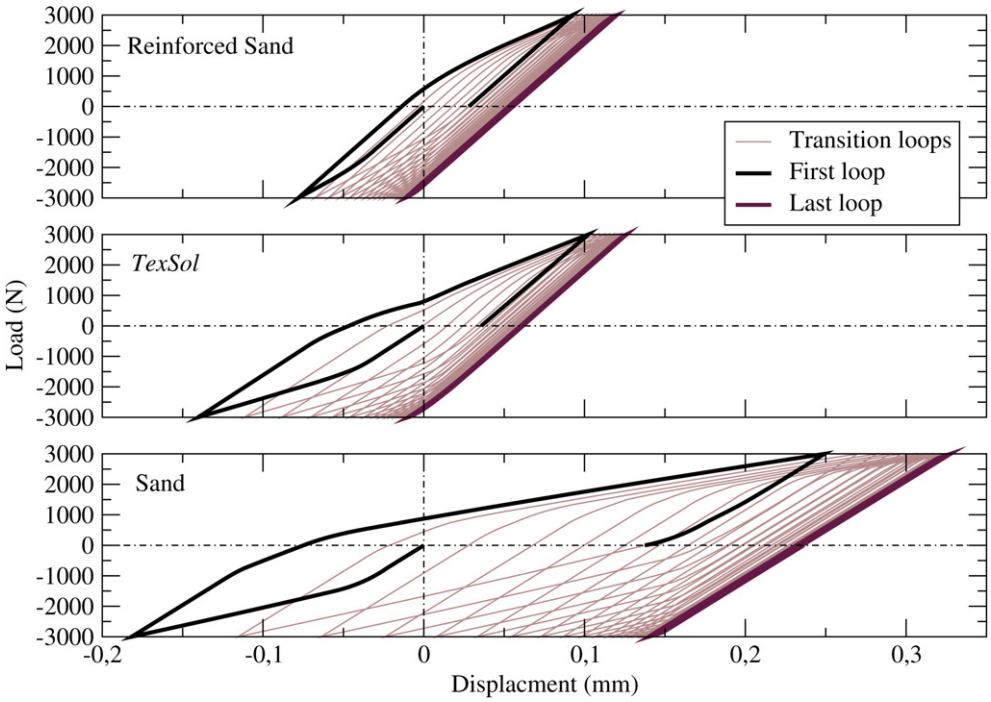

Fig. 11. Reinforced sand, *TexSol* and Sand behaviours on a cyclic test (20 compression traction load loops).

to apply a greater amplitude of loading on it: $\theta_f = 0.02$. *Reinforced sand*, *Texsol* and *Sand* cyclic behaviours are compared in Fig. 11. For the three models, the response tends to be stabilised after 20 cycles. But for *Reinforced sand* and *Texsol* the stabilisation is reached before 10 cycles. Moreover, the residual displacement of *Texsol* is close to that of *Reinforced sand* and five times smaller than that of *Sand*. This last result highlights the advantages of *TexSol* reinforcement. Another effect of the "unilateral" wire in the *Texsol* model is clearly illustrated by the curvature changes when the displacement switches sign from positive to negative.

4.4. Compression test

In soil mechanics, it is usual to carry out a triaxial test with a prescribed confinement pressure (cf. Fig. 12). Considering the previous numerical results of Section 4.2, the *Spherical Texsol* model is no more studied. Only the

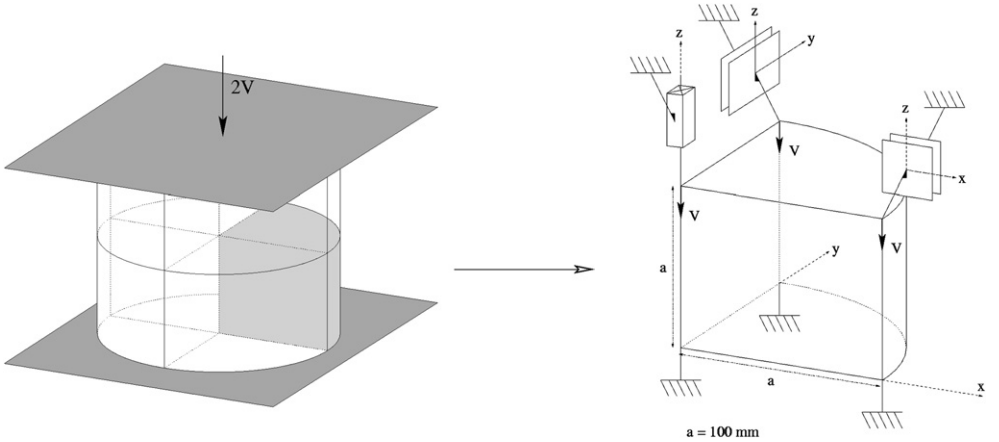

Fig. 12. Compression test.

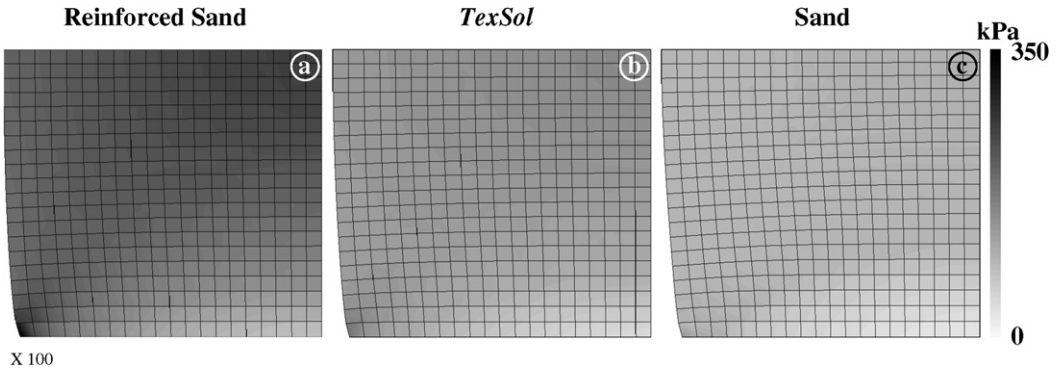

Fig. 13. Deviatoric stress.

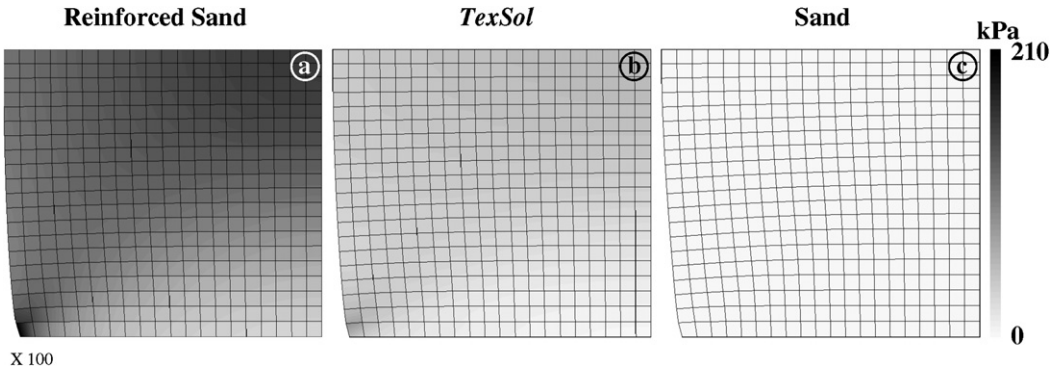

Fig. 14. Wire deviatoric stress.

three other cases are compared in a compression test (0.1 mm of vertical displacement computed in 100 iterations). The mesh is composed of 400 elements as described in (Laniel, 2004). We consider Q1-Lagrange hexahedron finite elements except for the central part which is meshed with R1-Lagrange pentahedron finite elements. The contribution of the wire in *TexSol* to the strength is illustrated by the spatial distribution of two stresses: the full stress $\boldsymbol{\sigma}$ and the wire stress $\boldsymbol{\sigma}_w$. The distribution of the full stress is identical in the three models with a level for *Texsol* which lies between the two others. The main part of stress is located at the center of the bulk except a localised concentration at the right lower corner. The contribution of the wire to the stress tensor ($\boldsymbol{\sigma}_w$) is split into its deviatoric and spherical (pressure) part. Both parts are identically zero for *Sand* (cf. Figs. 14(c) and 15(c)). The elasticity of the reinforcement is activated

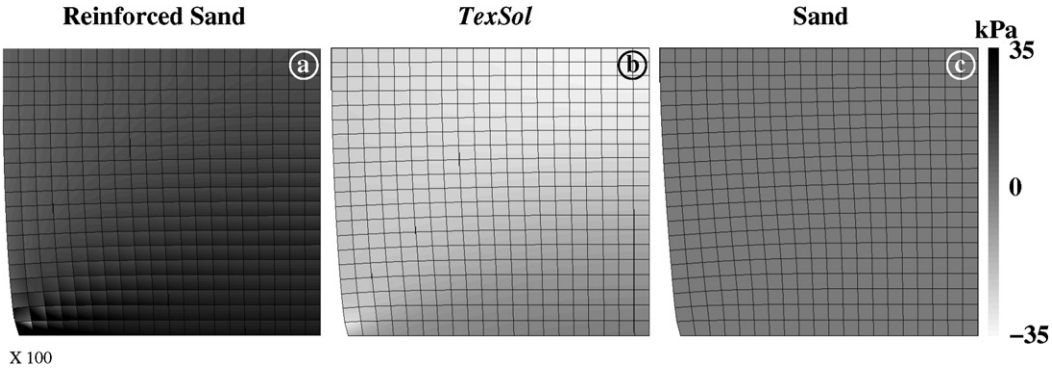

Fig. 15. Wire pressure.

only in tensile directions for *Texsol* and in all directions for *Reinforced sand*; this explains the difference in the levels of deviatoric stress for the total stress (Fig. 13) and for the wire stress (Fig. 14). The nature of the reinforcement due to wire is clearly illustrated in Fig. 15. Obviously, the wire pressure in the *Sand* sample vanishes. It is negative in the *Texsol* wire (traction behaviour) according to the unilaterality condition expressed in Eq. (21) whereas the pressure in the reinforcement of *Reinforced sand* is almost everywhere positive.

5. Conclusion and perspectives

In this paper a consistent thermodynamic model was proposed to account for numerical experiments (because of the absence of exploitable real experiments on *TexSol*). The key-point was the introduction of a "unilateral" elasticity which models the wire network. An elastic plastic model was superposed on the previous model to obtain both strain and stress formulations when it was possible. Using a finite element method, we validated qualitatively the expected behaviour.

The main perspective of this work is the identification of the mechanical parameters of the two-component model by numerical experiments which are currently underway. In a more general framework, it is useful to employ an orthotropic model for the wire network.

Acknowledgement

Thanks to Dr. Keryvin from the LARMAUR (Rennes) for his theoretic and logistics supports.

References

Cambou, B., Jean, M., 2001. Micromécanique des matériaux granulaires. Hermès Science, Paris.

Clarke, F.H., 1983. Optimization and Nonsmooth Analysis. Wiley-Interscience, New York;
Republished as Optimization and Nonsmooth Analysis. Classics in Applied Mathematics, vol. 5. SIAM, New York, 1990.

De Buhan, P., Sudret, B., 1999. A two-phase elastoplastic model for unidirectionally reinforced materials. Eur. J. Mech. A Solids 18, 995–1012.

Desrues, J., 2002. Limitations du choix de l'angle de frottement pour le critère de plasticité de Drucker–Prager. Rev. Fra. Gen. Civ. 6 (1), 853–862.

Drucker, D., Prager, W., 1952. Soil mechanics and plastic analysis of limit design. Quart. Appl. Math. 10, 157–165.

Dubois, F., Jean, M., 2003. LMGC90 une plateforme de développement dédiée à la modélisation des problèmes d'interaction. In: 6th CNCS Giens 1, pp. 111–118.

Fremond, M., 2002. Non-Smooth Thermo-Mechanics. Springer-Verlag, Berlin.

Halphen, B., Nguyen, Q.S., 1975. Sur les matériaux standards généralisés. J. Mécanique 14, 39–63.

Jean, M., 1999. The non smooth contact dynamics method. Computer Methods Appl. Mech. Engrg. 177, 235–257 (special issue).

Keryvin, V., 1999. Contribution à la modélisation de l'endommagement localisé. PhD Thesis, Université de Poitier, LMPM/LMA.

Khay, M., Gigan, J.-P., 1990. TEXSOL – Ouvrage de soutènement. LCPC.

Kichenin, J., Charras, T., 2003. CAST3M – Implantation d'une nouvelle loi d'évolution/loi de comportement mécanique. SEMT/LM2S, 2003.

Laniel, R., 2004. Simulation des procédés d'indentation et de rayage par éléments finis et éléments distincts. DEA, Université de Rennes I & INSA.

Laniel, R., Mouraille, O., Pagano, S., Dubois, F., Alart, P., 2005. Numerical modelling of reinforced geomaterials by wires using the non smooth contact dynamics. In: 4th CMIS, Hannover.

Leflaive, E., Khay, M., Blivet, J.-C., 1985. Un nouveau matériaux : le TEXSOL. Travaux, 602, pp. 1–3.

Lemaitre, J., Chaboche, J.-L., 1990. Mechanics of Solid Materials. Cambridge University Press, Cambridge.
Lucchesi, M., Pandovani, C., Pasquinelli, G., 2000. Thermodynamics of no-tension materials. Int. J. Solids Struct. 37, 6581–6604.
Moreau, J.-J., 1966. Fonctionnelles convexes. Séminaire Equations aux dérivés partielle, Collège de France.
Moreau, J.-J., 1999. Numerical aspects of the sweeping process. Comput. Methods Appl. Mech. Engrg. 177, 329–349.
Mouraille, O., 2004. Etude sur le comportement d'un matériau à longueur interne : le TexSol. DEA, Université de Montpellier II.
Radjaï, F., Preechawuttipong, I., Peyroux, R., 2001. Cohesive granular texture. In: Continuous and Discontinuous Modelling of Cohesive Frictional Materials, Vermeer, P.A., et al. (Eds.), pp. 149–162.
Simo, J.-C., Hugues, T.J.R., 1998. Computational Inelasticity. Springer-Verlag.
Suquet, P., 1982. Plasticité et homogénéisation. PhD Thesis, Université Pierre et Marie Curie, 1982.
Villard, P., 1988. Etude du renforcement des sables par des fils continus. PhD Thesis, Université de Nantes, ENSM.
Villard, P., Jouve, P., 1989. Behavior of granular materials reinforced by continuous threads. Computers and Geothechnics 7 (1–2), 83–98.
Wood, D.M., 1990. Soil Behaviour and Critical State Soil Mechanics. Cambridge University Press, Cambridge.
Yang, W.H., 1980. A generalized Von Mises criterion for yield and fracture. J. Appl. Mech. 47, 297–300.